

Mapping susceptibility of rainfall-triggered shallow landslides using a probabilistic approach

Chia-Nan Liu · Chia-Chen Wu

Received: 29 June 2007 / Accepted: 12 September 2007 / Published online: 3 October 2007
© Springer-Verlag 2007

Abstract To prepare a landslide susceptibility map is essential to identify hazardous regions, construct appropriate mitigation facilities, and plan emergency measures for a region prone to landslides triggered by rainfall. The conventional mapping methods require much information about past landslides records and contributing terrace and rainfall. They also rely heavily on the quantity and quality of accessible information and subjectively of the map builder. This paper contributes to a systematic and quantitative assessment of mapping landslide hazards over a region. Geographical Information System is implemented to retrieve relevant parameters from data layers, including the spatial distribution of transient fluid pressures, which is estimated using the TRIGRS program. The factor of safety of each pixel in the study region is calculated analytically. Monte Carlo simulation of random variables is conducted to process the estimation of fluid pressure and factor of safety for multiple times. The failure probability of each pixel is thus estimated. These procedures of mapping landslide potential are demonstrated in a case history. The analysis results reveal a positive correlation between landslide probability and accumulated rainfall. This approach gives simulation results compared to field records. The location and size of actual landslide are well predicted. An explanation for some of the inconsistencies is also provided to emphasize the importance of site information on the accuracy of mapping results.

Keywords Landslide · Rainfall · Mapping · Probability · Fluid pressure

List of symbols

c'	effective cohesion
D	index parameter for simulation accuracy
\bar{D}	normalized, d
D_o	diffusivity
FS	factor of safety
I	indicator function
$I_{R_{sim,i}}$	simulated reliability of pixel i
I_z	initial infiltration rate
K_z	conductivity
$N_{realization}$	number of realizations
P_F	failure probability
u	fluid pressure
Z	sliding depth
α	slope angle
ϕ'	effective friction angle

Introduction

Rainfall-triggered landslides are a recurring problem in Taiwan. They cause traffic disruption and economic damage or even claim catastrophic losses of human life. Therefore assessment of landslide susceptibility in specific areas is an important issue. A rational regional mapping for the susceptibility of rainfall-triggered landslides is especially necessary to provide information for the hazard reduction and community development, such as mitigation facilities, warning systems, regulation and management of land use, etc.

Landslide susceptibility zoning maps have been prepared using different methods, which can be grouped into statistical and analytical approaches. The statistical approach can be further divided into qualitative and

C.-N. Liu (✉) · C.-C. Wu
Civil Engineering Department, National Chi Nan University,
Nantou 545, Taiwan
e-mail: cnliu@ncnu.edu.tw

quantitative analyses. In qualitative analysis methods, such as the index method or the weighting method (Anbalagan and Singh 1996; Gupta and Anbalagan 1997; Saha et al. 2002; Ayalew et al. 2004), the various parameters and the relative significance of one parameter against another to the landslide are assigned by the users. The landslide potential is classified according to combination of these indices and weights. Therefore, qualitative methods have the disadvantage of subjectivity in assigning of indexes and weights based on the experience of experts. In quantitative analysis, the historical and observational data for landslides are collected as the dependent factors while several key variables contributing to these landslides are independent factors. Various statistical methods, such as bivariate analysis, multivariate statistical analysis (Carrara et al. 1991; He et al. 2003), or neural networks (Arora et al. 2004), have been employed. They are used to derive quantitative relationships between dependent and independent variables using linear or nonlinear models. The application of a quantitative approach provides objectivity over qualitative analysis. However, sufficient and accurate information about the landslide and contributing parameters are needed to construct this model. For example, Western et al. (2006) present concerns about the quality and quantity of landslide information for the generation of hazard zonation maps since such data are often limited in extent, imperfect or have variable quality. Thus the mapping results based on such data may lead to unreliable results. The analytical approach is usually conducted through slope stability analysis. The factor of safety of each pixel is calculated and combined together to map the distribution of severity for landslide hazards in the study region. For example, Luzi and Pergalani (1996), Pack et al. (1998), and Zhou et al. (2003) used infinite slope analysis and the ordinary slice method to generate slope stability maps for Italy, Canada, and Japan, respectively. On the other hand, some researchers build landslide hazard map probabilistically. For example, Coe et al. (2000) used Poisson probability model to analyze historical records of landslides for estimating the statistical properties of each pixel to build the landslide potential map. Chit et al. (2004) used historical landslides and rainfall data to estimate the annual probability of a 15-day accumulated rainfall exceeding the threshold value triggering a landslide. Zhou et al. (2003) considered the uncertainties in the soil strength properties to perform probabilistic analysis for potential slope failures.

There are many sources of uncertainty associated with mapping landslide susceptibility. For example, the accuracy of information about past landslides and contributing parameters (elevation, slope angle, aspect, rainfall, etc) for the statistical approach is significantly dependent on the precision and version of remote sensing results. The

parameters (strength properties, pore water pressure, failure surface, etc) applied in an analytical approach for estimating the factor of safety for slopes are also inherently spatially heterogeneous. Thus, the quality and quantity of available data affect the exactness of generated landslide hazard map. A deterministic map showing the spatial distribution of level (class, or factor of safety, etc) of landslide hazard is not sufficient to consider these uncertainties. For showing landslide occurrence potential (or probability), it is more appropriate to use a map that includes the spatial and temporal uncertainties of the data used for the map generation. The goal of this study is to conduct probabilistic analysis to evaluate the probability of landslide occurrence triggered primarily by rainfall. In this paper, the analysis procedures include the application of analytical method, calculation of factor of safety, conduction of Monte Carlo simulation, evaluation of slope failure probability, and generation of hazard map. The landslide susceptibility map of a case site is built to demonstrate the manipulation of proposed methodology.

Methodology

The approach of mapping regional landslide hazards begins by calculating the factor of safety of each pixel. The Monte Carlo method is incorporated in the calculation of factor of safety by multiple simulations until the failure probability of each pixel is obtained. The simulation process of evaluating the failure probability of each pixel in the study region is flow charted in Fig. 1. The details of performing stability analysis and simulation are presented in this section.

Mapping factor of safety using TRIGRS

Transient rainfall infiltration and grid-based regional slope-stability (TRIGRS), developed by the USGS (Baum et al. 2002), is a Fortran program to estimate the spatial and temporal distribution for the factors of safety over a study region. TRIGRS uses the simplified analytical solution of Richard's equation developed by Iverson (2000) to calculate the fluid pressure distribution within a slope during rainfall. The total fluid pressure, u , is superimposed by steady and transient pressures. In TRIGRS the study region is divided into multiple square pixels, which are independent from each other. The factor of safety for each pixel is calculated using the infinite slope method. The factors of safety for all pixels are combined to present a spatial distribution of the factors of safety over the study region. TRIGRS also has features to include a heterogeneous distribution of mechanical and hydrological properties, and to

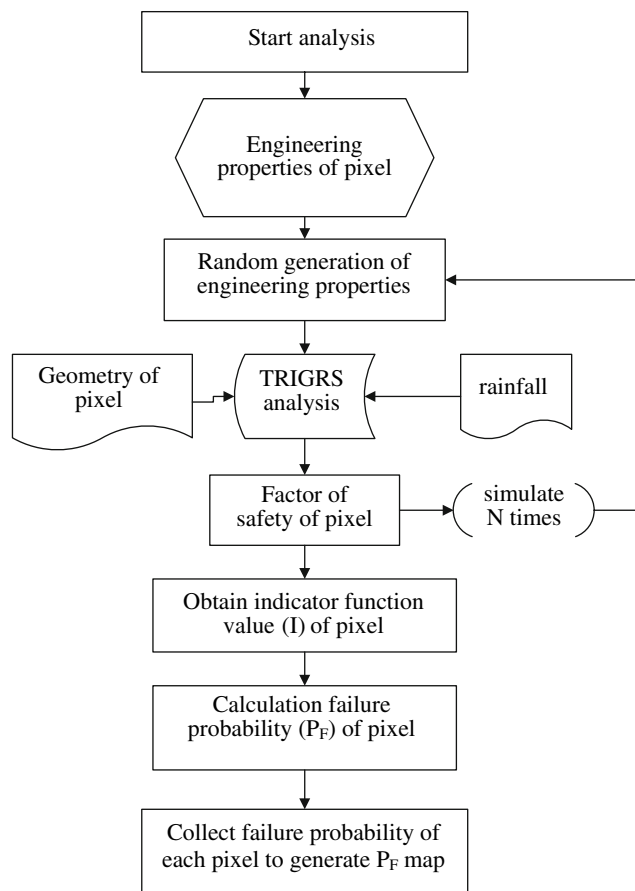


Fig. 1 The process of building the regional failure probability map in the study

calculate spatial and temporal distribution of fluid pressure within the slope. With these features, it is becoming a popular numerical code for rainfall-induced landslide hazard mapping. For example, Baum et al. (2005) used TRIGRS to study the temporal correlation of factor of safety, pore water pressure, failure time and rainfall duration of a failure case in Seattle. Similarly, Chen et al. (2005) also used TRIGRS to generate a spatial landslide susceptibility map of Tienliao in Taiwan.

Monte Carlo simulation of slope failure probability

The factor of safety is an index of the level of stability. The intent of a factor of safety is to account for uncertainty in design and analysis. Uncertainty in a factor of safety arises from uncertainty in the individual variables. The sources of uncertainties include shear strength (c' , ϕ'), the fluid pressure (u), the unit weight of soil (γ), slope angle (α), and sliding depth (Z). Furthermore, the uncertainty in fluid pressure comes from uncertainties in conductivity (K_z), diffusivity (D_o), and initial infiltration rate (I_z). Therefore,

the actual landslide reliability is not known from a deterministic value due to uncertainty in the calculation of factor of safety.

Monte Carlo simulation repeatedly samples values from the probability distributions for the uncertain variables then puts them into a model to calculate the corresponding outcome. It is a useful tool to approximate the probability when the analytical results are difficult to obtain. For example, Liu and Chen (2006) applied it to simulate the spatial distribution of CPT measurement to map the liquefaction potential over Yuanlin town in Taiwan. Monte Carlo simulation is also popular for mapping slope stability. For example, Zhou et al. (2003) used it to simulate the strength parameters to build a map of landslide probability. Wang et al. (2006) used 3D slope-stability analysis models and Monte Carlo simulation to identify the locations of potential landslides.

In this analysis, the Monte Carlo simulation technique is implemented into the TRIGRS program. The mean value and variance of random variables of each element are input to form a specific probability distribution. The information of mean value and standard deviation is to provide both the most possible value of a variable and its variation. Randomly sampled values from these probability distributions along with deterministic variables are input into TRIGRS to calculate the fluid pressures as a function of time and location, while the factor of safety of each pixel corresponding to these parameters is calculated in the infinite slope approach. The procedures for generating random numbers, calculation of fluid pressures, and evaluation of factor of safety, are repeated many times in one set of Monte-Carlo simulations. The failure probability for pixel i , $P_{F,i}$, is calculated from the simulation results as follows:

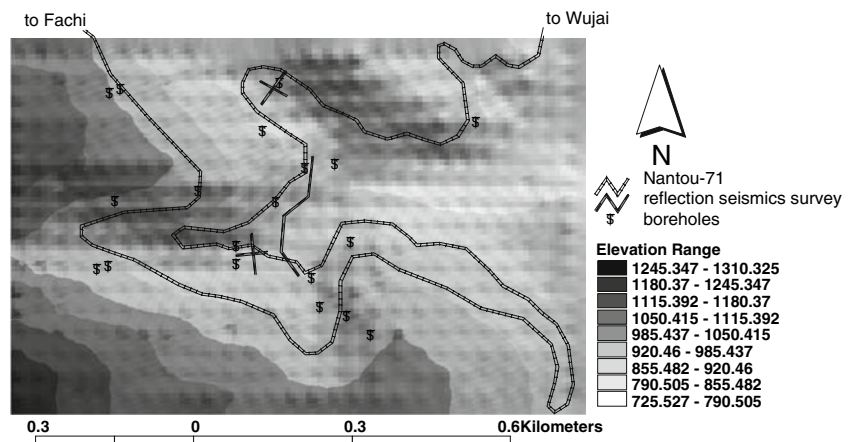
$$P_{F,i} = \left(\sum_{j=1}^{N_{\text{realization}}} I_j \right) / N_{\text{realization}} \tag{1}$$

where $N_{\text{realization}}$ is the number of realizations conducted; I_j is an indicator function with a value of 1.0 if the factor of safety is smaller than unity and a value of 0.0 otherwise.

Landslide susceptibility map: case study

Route Nantou 71 is in the central Taiwan. The section between the WuJai tribe and Fachi village (Fig. 2) suffered severe damage due to landslide during Typhoon Toraji on 30/07/2001. The hourly rainfall histogram along with accumulated rainfall of this storm is shown in Fig. 3. The landslides in that section were characterized as shallow, planar slope failure. The landslide susceptibility of this region corresponding to this storm event will be mapped using the approach proposed in this study. The study area

Fig. 2 The terrain map of study region, locations of investigation boreholes and reflection seismic survey



covers a region of about 1 km^2 ($1,120 \text{ m} \times 720 \text{ m}$). According to the geological map provided by the Central Geological Survey, this area is composed of Chiayuan formations. The regional geological context is not complex. Field observations and investigation borehole logs reveal that the site is overlain by weathered residual soil, which is derived from strong weathering process. Immediately underneath this loose compacted residual soil are colluvium deposits and less weathered slates mixed with sandstone and siltstone. The colluvium originated from the previous landslides. This layer is underlain by fresh, unweathered rock formations. The terrain map of this study region is shown in Fig. 2, indicating that hillslopes in the study area are moderate to steep.

Preparing data for analysis

Several investigations were done to collect the soil properties, hydrologic and geological information. After the landslides occurred on 30/07/2001, a total of 21 geotechnical investigation boreholes were drilled and 5 reflection seismic surveys along 5 profiles (total length is 460 m) were conducted for site exploration. The locations of investigation boreholes and profiles are shown in Fig. 2. Data from investigation boreholes confirms the geological stratification of the study region is composed of topsoil, colluvium and weathering layer, and rock. The topsoils and weathered layer deposits on the rock surface to varying thickness, generally between 1 and 16 m. The soil specimens sampled from different depths of each borehole were brought back to laboratory for direct shear testing to estimate the shear strength parameters (c' and ϕ'). There were 21 specimens each for topsoil, colluvium and weathering layer, and rock layer. The mechanical test results are shown in Table 1. It can be noted there is some variation in the test results, especially for the colluvium and weathering layers. This variation was attributed to heterogeneity in the

colluvium, and this variation has also been reported by others (Luzi and Pergalani 1996; Duncan 2000; Thurner and Schweiger 2000; Refice and Capolongo 2002; Zhou et al. 2003). The reported coefficients of variation (cov) in the unit weight, friction angle, and cohesion are 3–7, 2–20, and 5–30%, respectively.

Despite some variation in the test results, they indicate the unweathered rock formation is stronger than the topsoils, weathering rock and colluvium. It is reasonable to assume a failure triggered by rainfall would be located within the weaker, more permeable stratifications. The location of interface between fresh rock and the overlying loosely packed layers at the site investigation (including boreholes and reflection seismic tests) site was identified based on the exploration profiles. These depths were interpolated to prepare the spatial distribution of fresh rock surface. Because the study region is very mountainous (as shown in Fig. 2), the interpolated profile of the rock surface presented some unreasonable results, such as the elevation of rock surface being above the ground surface.

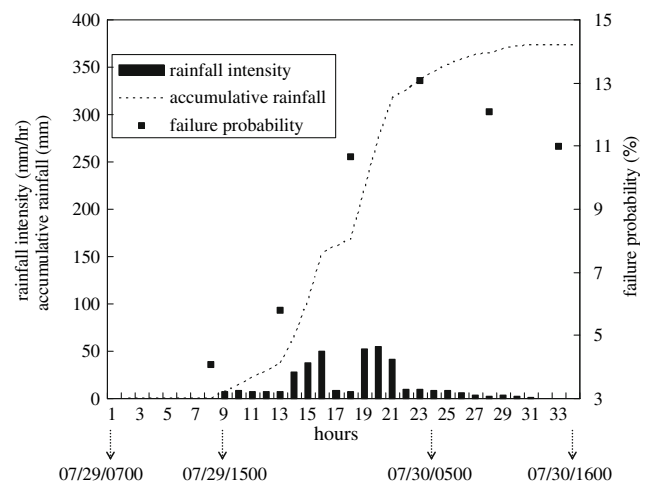


Fig. 3 Hourly rainfall histogram (2001/07/29/0700–2001/07/30/1600) of Typhoon Toraji

Table 1 Mechanical properties of geological stratification

Type	Unit weight (kN/m ³)	<i>c'</i> (kPa)	ϕ' (°)
Top soil	19.8–20.4	0–20	25
Colluvium and weathering layer	20.4–26.1	20–98	25–40
Rock	26.1–26.8	294	25

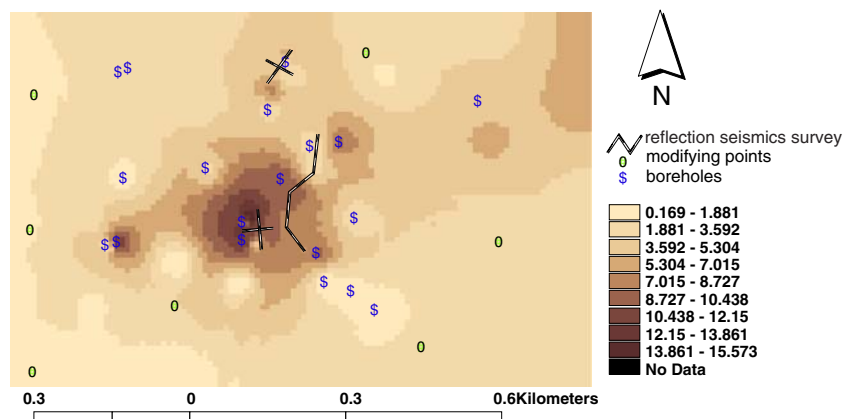
This happened mostly at locations far from the site investigation points, i.e., far away from the reference points. This defect was corrected, according to the approach presented in Chen et al. (2005), by adding some reference points located at hilltops. The thickness of topsoil and colluvium at these modifying points were assumed to be small since the loosely packed soil material tends to slide down from slope top. The thickness of loosely packed soil layers was calculated as the difference of the elevation between ground surface and rock surface. Figure 4 shows a map of the estimated thickness of loosely packed soil layer over the study region. About 90% of the slopes had a sliding thickness less than 6 m. That is, most of the slopes can be characterized with pattern of shallow slope failure.

The groundwater table was observed from 11 monitoring wells (adopted from some boring holes) over 1 year. The long-term observation data showed the ground water table was usually between 25 and 39 m below the ground surface, which is much deeper than the potential sliding surface. This indicates the long-term ground water table (i.e., steady fluid pressure) has no adverse influence on the shallow slope stability discussed in this study. However, perching water is expected to form during a heavy rainfall on the interface of a permeable loosely packed soil layer and the underlying rock that is more intact and less permeable. This perching water adds fluid pressure to the potential sliding surface. It responds purely to the infiltration and its effect is transient. Therefore, only the transient fluid pressure calculated using TRIGRS will influence the stability analysis of infinite slope. For simplicity, the

groundwater table was assumed to be located at the same level as the elevation between ground surface and rock surface.

The hydrological parameters (conductivity K_z , diffusivity D_o , and initial infiltration rate I_z) are important factors affecting the transient fluid pressure. The values of hydraulic conductivity and diffusivity for colluvium and weathered soil layer collected from the literature are listed in Table 2. The hydraulic conductivity ranges between 1.2×10^{-6} and 1×10^{-3} since it is dependent on the size and percentage of voids, fine content, soil density, etc. These properties substantially differ from sample to sample and are site specific. Therefore the range of hydraulic conductivity listed in Table 2 is wide. Besides, because of the very complex composition of soil particles, it is difficult to retrieve a representative sample from a very heterogeneous field. Thus it is not easy to conduct a satisfactory permeability test on colluvium, even for different soils sampled from the same site. For example, as shown in Table 2, the cov in the hydraulic conductivity reported by Gui et al. (2000) and by Montgomery et al. (2002) is 31 and 76%, respectively. The reported diffusivity values also range widely, between 1×10^{-2} and 5×10^{-5} . In this study, it is observed that the value of diffusivity is about 10–500 times the value of hydraulic conductivity, and so the D_o value is assumed to be 200 times the K_z of soil. References to initial infiltration (I_z) rate are scarce in the literature. Generally, the concept is that this parameter describes the soil moisture condition. If the soil is saturated, it can be assumed to be the same as hydraulic conductivity, while this value can be 0 for the soil in a very arid region. However, the discrepancy is still significant in defining its value even for regions with similar climates. For example, Zhou et al. (2003) set this value to be 0 for a slope in Hong Kong while Chen et al. (2005) set this value as the hydraulic conductivity for a case study in Taiwan. The rainfall record of the WuJai station showed there was not much rain before Typhoon Toraji (130 mm for the

Fig. 4 Spatial distribution of thickness of loosely packed soil layer



preceding 40 days) so the soil was probably dry at the beginning of rainfall. Therefore the I_z can reasonably be assumed to be 0.01 of the K_z for soil in this study. These hydrological parameters are assumed to be uniform and homogeneous within the loosely packed soil layer above the sliding surface. The spatial and temporal distribution of transient fluid pressure corresponding to the rainfall event of Typhoon Toraji (Fig. 3) was calculated using the TRIGRS program for further slope stability analysis.

To prepare the landslide susceptibility map, the study region was divided into pixels. The study area is meshed into 8,064 pixels for landslide potential mapping. The dimension of each pixel is 10 m (length) \times 10 m (width). The data layers of potential sliding depth and fluid pressure, as described in the previous paragraphs, were prepared for the GIS system to capture values for each pixel. Digital elevation model data were used to lay out the topographical parameters. For more accurate calculations, the original 40 m \times 40 m digital elevation model (DEM) published by the Agriculture and Forestry Aerial Survey Institute in 1994 was refined to 10 m \times 10 m by using the inverse distance weighting (IDW) model that is embedded in Arcview 3.2.

The attributes and statistical properties of parameters input for analysis are listed in Table 3. The shear strength parameters (c' , ϕ') and soil unit weight (γ) were treated as normally distributed random variables (Lumb 1966). The hydraulic conductivity (K_z) was treated as lognormally distributed random variables (Freeze 1975; Hoeksema and Kitanidis 1985; Sudicky 1986; Yang et al. 1996). As described in the previous section, initial infiltration rate (I_z) and diffusivity (D_o) were assumed to be 0.01 and 200 of K_z . Therefore their probabilistic distributions were also log-normal. The slope angle and sliding surface were assumed to be deterministic but not homogeneous. Since they were spatially distributed over the study region, the potential failure surface and slope angle were different for

each pixel. These values were captured from data layers (Figs. 4, 5) by using a GIS system. Though the statistical properties of each parameter listed in Table 3 refer to the test results, site investigation results, and information collected from previous researches, it is noteworthy that certain extent of uncertainty exist in these parameters because of the insufficiency, subjective judgment or even errors in the process of data preparation. The effects of these design parameters on the landslide susceptibility will be discussed later.

Mapping slope failure susceptibility over study region

Following the procedures presented in Fig. 1, randomly generated numbers were assigned into the cumulative density function of c' , ϕ' , γ , and K_z to generate the values for these random variables and corresponding I_z and D_o variables. These hydrological parameters along with the topographical data of each pixel, and the hourly rainfall histogram recorded in WuJai station (Fig. 3) were input into the TRIGRS program to simulate the resultant spatial distribution of transient fluid pressure. The infinite slope method imbedded in TRIGRS was used to calculate the factor of safety of landslide of each pixel for this realization. The simulated statistical estimators of four random variables, c' , ϕ' , γ , and K_z for different number of simulations (N) are compared with the input statistical properties. The results show that 2,000 simulations are appropriate for the N value in this analysis. Therefore the above procedures for evaluating factor of safety in all pixels were repeated for 2,000 realizations. The 2,000 factors of safety of each pixel were collected to calculate the failure potential by using Eq. 1. It should be noted the temporal distribution of temporal fluid pressure can be estimated, so the calculation of landslide potential of study area during rainfall is also feasible.

Table 2 Ranges of hydraulic conductivity and diffusivity for colluvium and weathered soil layer

Reference	Hydraulic conductivity [cov] (m/s)	Diffusivity (m^2/s)
Gui et al. (2000)	2.9×10^{-6} [31%]	–
Iverson (2000)	1×10^{-4}	1×10^{-3}
Montgomery et al. (2002)	1×10^{-4} [76%]	–
Lancaster et al. (2002)	1×10^{-3} – 1×10^{-4}	3.2×10^{-3}
D'Odorico et al. (2005)	1×10^{-5}	1×10^{-3}
Lan et al. (2005)	1.5×10^{-4} – 1.2×10^{-6}	7×10^{-2} – 6×10^{-4}
Baum et al. (2005)	1×10^{-5} – 5×10^{-5}	1×10^{-4} – 5×10^{-5}
Chen et al. (2005)	1×10^{-4} – 1×10^{-5}	1×10^{-2}

Table 3 Characteristic of design parameters in this study

Parameter (unit)	Type	Mean value	Cov (%)
Cohesion, c' (kPa)	Normal	24.5	7
Friction angle, ϕ' (kPa)	Normal	30	18
Soil unit weight, γ (kN/m ³)	Normal	19.6	2.5
Hydraulic conductivity, K_z (m/s)	Log-normal	10^{-4}	74
Initial infiltration rate, I_z (m/s)	Log-normal	$0.01 K_z$	–
Diffusivity, D_o (m^2/s)	Log-normal	$200 K_z$	–
Sliding surface, Z (m)	Deterministic	Fig. 4	–
Slope angle, α ($^\circ$)	Deterministic	Fig. 5	–

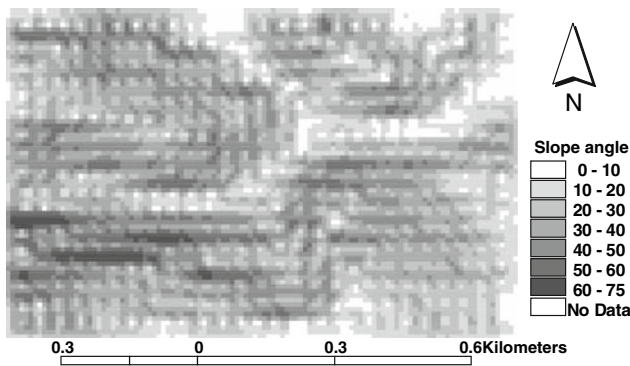


Fig. 5 The spatial distribution of slope angle of study region

The failure probability over the study region corresponding to 0, 5, 10, 15, 20, and 25 h subsequent to the initiation (2001/07/29/1500) of the Typhoon Toraji rainfall event is shown in Fig. 6. It shows the initial state of this region is generally stable. The area ratios for failure probability (P_F) smaller than 10%, between 10 and 50%, and larger than 50%, are about 93, 4, and 3%, respectively. As the rainfall begins, landslide susceptibility begins to increase. The area ratio for very stable ($P_F < 10\%$) pixels decreases while the area ratio for unstable pixels increases. The increase of area ratio is more significant for the pixels of higher failure potential. For example, after 15 h of rainfall, the area ratios for failure probability between 50 and 90%, and larger than 90%, increase by 4 and 6%, respectively. The average failure probability over the whole study region was calculated and plotted versus the rainfall histogram (Fig. 3) to show the positive correlation between accumulated rainfall and failure susceptibility. This trend changes 15 h after the initiation of rainfall. The decreased failure probability results from the decrease of transient fluid pressure after most of the intense rainfall had occurred during the 15 h span. The landslide potential map of 0 and 15 h after rainfall are shown in Fig. 7 to

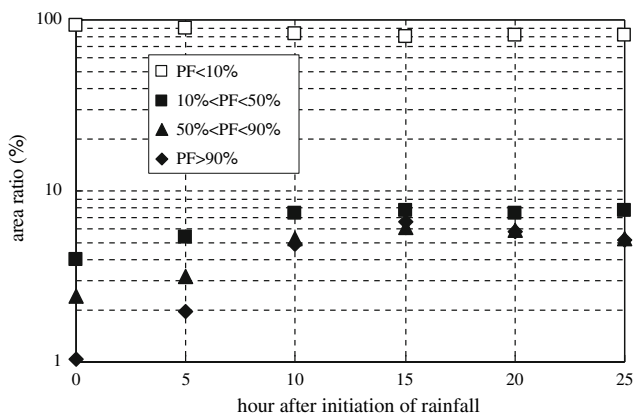


Fig. 6 Failure probability of pixels over the study region during the Typhoon Toraji rainfall event

illustrate the comparison of landslide potential susceptibility between the status prior to the rainfall and the most critical status triggered by the rainfall.

The landslide potential map at 15 h after rainfall initiation is compared with the field records of landslides triggered by this rainfall event (Fig. 8). It shows that locations of clusters of higher landslide potential are comparable to the location and shape of the observed landslide phenomena after Typhoon Toraji. The average landslide probability for the 911 pixels in which a landslide did occur is 48.4%, while it is only 8.8% for the 7,153 pixels in which a landslide did not occur. To quantitatively compare the simulated landslide potential, an index parameter D is introduced. D is defined as the total least square of the difference between the simulated landslide potential and the observed landslide phenomena (Fig. 8):

$$D = \sum_{i=1}^n (I_{R_{sim,i}} - I_{R_{obs,i}})^2 \quad (2)$$

where $I_{R_{sim,i}}$ is the simulated reliability of pixel i , and $I_{R_{obs,i}}$ is the observed reliability of pixel i . Corresponding to the field observed phenomena at grid I , $I_{R_{obs,i}}$ is set to be zero and 1.0, respectively. The D value can be normalized as \bar{D} by the number of pixels (n). A smaller \bar{D} value indicates that the simulated landslide potential distribution compares better with field observation, and vice versa. The \bar{D} values for the landslide probability map corresponding to 15 h after the initiation of rainfall is 0.04. This value quantitatively indicates the mapping results compare very well with field observations.

Discussion and conclusions

This paper provides a practical approach for mapping landslide susceptibility of each pixel in an area. Compared with the defects of subjectivity embedded in qualitative approaches and the imperfect or limited historical landslide data in quantitative approaches, this approach is based on solid consideration of analytical analysis. The study region was meshed into pixels and the important random parameters were simulated according to their statistical characteristics. The temporal and spatial distribution of transient fluid pressure was evaluated using Richard’s equation by synthesizing the information on hydrological parameters, topography, and rainfall data. The factor of safety of each pixel is calculated by using the infinite slope method with the inputs of fluid pressure, strength parameters, and geometrical data. Monte Carlo simulation is implemented into the TRIGRS program to conduct multiple simulations of factor of safety and thus to evaluate the corresponding failure

Fig. 7 The landslide potential map of study area corresponding to 0 (above) and 15 h (below) subsequent to the initiation of rainfall

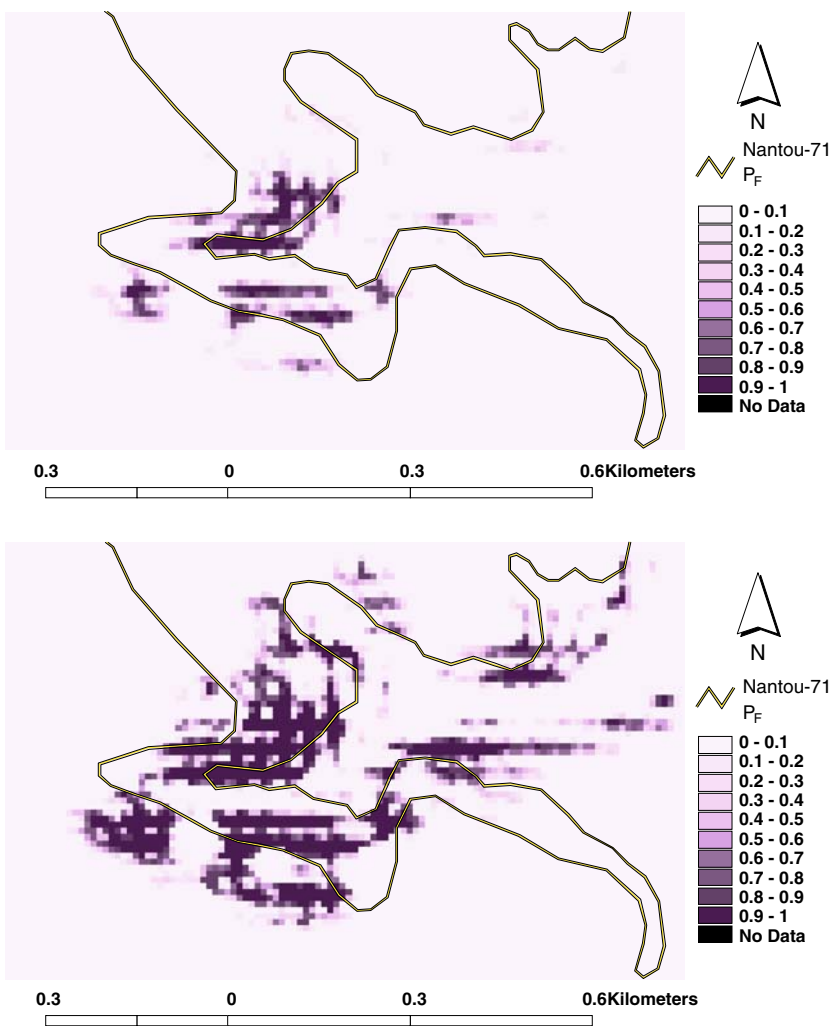


Fig. 8 Comparison between the most critical (2001/07/30/0500) status of simulated landslide probability of study area and field records of landslides



probability. A case history of landslides actually triggered by Typhoon Toraji in Taiwan was used to demonstrate how to manipulate the approach. It shows the landslide probability over the study region increasing with the accumulation of rainfall. The simulated potential map is generally comparable to the field observations. The landslide probability map

built in this study is superior to the map built by using a factor of safety approach in the following aspects: (1) it gives more detailed information regarding locations and potential for landslides (2) it consider uncertainty in the parameters contributing to a landslide, and (3) it provides the failure probability to do quantitative analysis of reliability-based

risk evaluation and decision-making for mitigation and emergency measures.

There are two main limitations in the approach proposed in this study. Firstly, significant changes may have occurred to the terrain because some slopes on this site are prone to be unstable. Therefore the precision of available aerial photos and digital elevation model are of questionable. The second limitation is the justification of infinite slope assumption. It is noteworthy the proposed approach is valuable only when updated remote sensing maps can be applied on appropriate sites which satisfy the characteristics of infinite slope.

References

Anbalagan R, Singh B (1996) Landslide hazard and risk assessment mapping of mountainous terrains—a case study from Kumaun Himalaya, India. *Eng Geol* 43:237–246

Arora MK, Das Gupta AS, Gupta RP (2004) An artificial neural network approach for landslide hazard zonation in the Bhagirathi (Ganga) Valley, Himalayas. *Int J Remote Sens* 25:559–572

Ayalew L, Yamagishi H, Ugawa N (2004) Landslide susceptibility mapping using GIS-based weighted linear combination, the case in Tsugawa area of Agano River, Niigata Prefecture, Japan. *Landslides* 1:73–81

Baum RL, Savage WZ, Godt JW (2002) TRIGRS—a Fortran program for transient rainfall infiltration and grid-based regional slope-stability analysis. In: U.S. geological survey open-file report 02–424

Baum RL, Coe JA, Godt JW, Harp EL, Reid ME, Savage WZ, Schulz WH, Brien DL, Chleborad AF, McKenna JP, Michael JA (2005) Regional landslide-hazard assessment for Seattle, Washington, USA. *Landslides* 2(4):266–279

Carrara AM, Cardinali M, Detti R, Guzzetti F, Pasqui V, Reichenbach P (1991) GIS techniques and statistical models in evaluating landslide hazard. *Earth Surf Process Landforms* 16:427–445

Chen CY, Chen TC, Yu FC, Lin SC (2005) Analysis of time-varying rainfall infiltration induced landslide. *Environ Geol* 48:466–479

Chit KK, Flentje P, Chowdhury R (2004) Interpretation of probability of landsliding triggered by rainfall. *Landslides* 1:263–275

Coe JA, Michael JA, Crovelli RA, Savage WZ (2000) Preliminary map showing landslide densities, mean recurrence intervals, and exceedance probabilities as determined from historic records, Seattle, Washington. In: USGS open-file report 00-303, on-line edition

D’Odorico P, Fagherazzi S, Rigon R (2005) Potential for landsliding: Dependence on hypsograph characteristics. *J Geophys Res* 110:F01007. doi:10.1029/2004JF000127

Duncan JM (2000) Factors of safety and reliability in geotechnical engineering. *J Geotech Geoenviron Eng* 126:307–316

Freeze RA (1975) A stochastic-conceptual analysis of one-dimensional groundwater flow in nonuniform homogeneous media. *Water Resour Res* 11:725–741

Gui SX, Zhang R, John PT (2000) Probabilistic slope stability analysis with stochastic soil hydraulic conductivity. *J Geotech Geoenviron Eng* 126:1–9

Gupta P, Anbalagan R (1997) Slope stability of Tehri Dam reservoir area, India, using landslide hazard zonation (LHZ) mapping. *Eng Geol* 30:27–36

He YP, Xie AH, Cui AP, Wei AFQ, Zhong ADL, Gardner AJS (2003) GIS-based hazard mapping and zonation of debris flows in Xiaojiang Basin, southwestern China. *Environ Geol* 45:286–293

Hoeksema RJ, Kitanidis PK (1985) Analysis of the spatial structure of properties of selected aquifers. *Water Resour Res* 21:563–572

Iverson RM (2000) Landslide triggering by rain infiltration. *Water Resour Res* 36:1897–1910

Lan HX, Lee CF, Zhou CH, Martin CD (2005) Dynamic characteristics analysis of shallow landslides in response to rainfall event using GIS. *Environ Geol* 47:254–267

Lancaster ST, Hayes SK, Grant GE (2002) Modeling sediment and wood storage and dynamics in small mountainous watersheds. *Geomorphic Processes Riverine Habitat Water Sci Appl* 4:85–102

Liu CN, Chen JH (2006) Mapping liquefaction potential considering spatial correlations of CPT measurements. *J Geotech Geoenviron Eng* 132:1178–1187

Lumb P (1966) The variability of natural soils. *Can Geotech J* 3:74–97

Luzi L, Pergalani F (1996) Applications of statistical and GIS techniques to slope instability zonation (1:50000 Fabriano geological map sheet). *Soil Dyn Earthquake Eng* 15:83–94

Montgomery DR, Dietrich WE, Heffine JT (2002) Piezometric response in shallow bedrock at CB1:Implications for runoff generation and landsliding. *Water Resour Res* 38(12):1274. doi:10.1029/2002WR001429

Pack RT, Tarboton DG, Goodwin CN (1998) The SINMAP approach to terrain stability mapping. In: Proceedings of 8th congress of the international association of engineering geology, pp 1157–1165

Refice A, Capolongo D (2002) Probabilistic modeling of uncertainties in earthquake-induced landslide hazard assessment. *Comput Geosci* 28:735–749

Saha AK, Gupta RP, Arora MK (2002) GIS-based landslide hazard zonation in the Bhagirathi (Ganga) Valley, Himalayas. *Int J Remote Sens* 23:357–369

Sudicky EA (1986) A natural gradient experiment on solute transport in a sand aquifer: spatial variability of hydraulic conductivity and its role in the dispersion process. *Water Resour Res* 22:2069–2083

Thurner R, Schweiger HF (2000) Reliability analysis for geotechnical problems via finite elements—a practical application. *Extended Abstracts Int Conf Geotech and Geol Eng Aust Melbourne* 11:1–6

Wang C, Esaki T, Xie M, Qiu C (2006) Landslide and debris-flow hazard analysis and prediction using GIS in Minamata–Hou-gawachi area, Japan. *Environ Geol* 51:91–102

Western van CJ, Asch van TWJ, Soeters R (2006) Landslide hazard and risk zonation—why is it still so difficult?. *Bull Eng Geol Environ* 65:167–184

Yang J, Zhang R, Wu J, Allen MB (1996) Stochastic analysis of adsorbing solute transport in two-dimensional unsaturated soil. *Water Resour Res* 32:2747–2756

Zhou G, Esaki T, Mitani Y, Xie M, Mori J (2003) Spatial probabilistic modeling of slope failure using an integrated GIS Monte Carlo simulation approach. *Eng Geol* 68:373–386